

Article

# Nonlinear Modeling and Analysis of Wound-Rotor Synchronous Starter/Generator (WRSSG) in Generating State for More Electric Aircraft

Haoran Du <sup>1</sup> , Yongzhi Liu <sup>2,\*</sup>, Tianxing Li <sup>2</sup> and Peirong Zhu <sup>1</sup><sup>1</sup> Graduate School, Air Force Engineering University, Xi'an 710038, China; duhaoran19991008@163.com (H.D.)<sup>2</sup> Aviation Engineering School, Air Force Engineering University, Xi'an 710038, China

\* Correspondence: Liuyz\_kj@163.com

**Abstract:** The nonlinear modeling and analyzing of wound-rotor synchronous starter/generators (WRSSGs) plays a vital role in the analysis and monitoring of aircraft power systems. Moreover, they are of great significance with regard to the establishment of a future aircraft smart grid. However, owing to its nonlinear, high-dimensional, and strong coupling characteristics, this modeling has always remained in the frequency domain stage and the progress of more intuitive time domain modeling has been slow. This paper presents a nonlinear model of a WRSSG in a generating state. When the WRSSG is in power generation mode, most cases indicate that the aircraft is in flight mode. The establishment of the nonlinear model of the system in the power generation state is of great significance for the research of the health management and state monitoring of the aircraft power system and can improve the safety and reliability of the aircraft during flight. The model uses FE analysis and neural network to solve the nonlinear problem of the motor in the system and uses the improved variable parameter average model to solve the nonlinear problem of the rotating rectifier. According to the principle of signal transmission, a time domain model for the whole system is developed. Finally, the model is compiled by the RT-LAB real-time simulator. The nonlinear model performs well when compared with FE analysis results and tested against the MIL-STD-704F standard. The proposed nonlinear model and analysis results can be used for the condition monitoring and fault diagnosis of aircraft power systems. The hardware-in-the-loop test platform based on an accurate nonlinear model is a feasible means to study the failure of expensive equipment, and it can aid the study of irreversible failures of equipment at a low cost.

**Keywords:** condition monitoring; more electric aircraft (MEA); nonlinear modeling; wound-rotor synchronous starter/generator (WRSSG); hardware-in-the-loop



**Citation:** Du, H.; Liu, Y.; Li, T.; Zhu, P. Nonlinear Modeling and Analysis of Wound-Rotor Synchronous Starter/Generator (WRSSG) in Generating State for More Electric Aircraft. *Actuators* **2023**, *12*, 439. <https://doi.org/10.3390/act12120439>

Academic Editor: Ignazio Dimino

Received: 14 October 2023

Revised: 22 November 2023

Accepted: 23 November 2023

Published: 25 November 2023



**Copyright:** © 2023 by the authors. Licensee MDPI, Basel, Switzerland. This article is an open access article distributed under the terms and conditions of the Creative Commons Attribution (CC BY) license (<https://creativecommons.org/licenses/by/4.0/>).

## 1. Introduction

In recent years, the concept of the more electric aircraft (MEA) has developed rapidly. As a type of secondary energy for aircrafts, electric energy has the characteristics of low emissions, low cost, and high stability, which other secondary energy sources do not possess. Electrical energy accounts for an increasing proportion of the types of secondary energy in aircrafts [1,2]. Moreover, MEAs will be an inevitable trend of future aircraft development in both the civil and military fields. For example, the Boeing 787 and Airbus A380 (civil) and the F-35 (military) are outstanding representatives of more electric aircrafts [3–5].

WRSSGs play a crucial role in aircraft power systems. From the perspective of future developments in aircraft electrical power systems (EPSs), there are four possible options [6]:

- EPS-A1: constant frequency AC EPS (115 V/400 Hz AC);
- EPS-A2: hybrid AC and DC EPS (115 V/360–800 Hz AC and 270 V DC);
- EPS-A3: hybrid HVAC and HVDC EPS (230 V/360–800 Hz AC and  $\pm 270$  V DC);
- EPS-A4: pure HVDC EPS ( $\pm 270$  V DC).

Regardless of whether it is an AC or HVDC power generation system, the WRSSG represents their best choice. This system can be directly used as an AC power generation system and can be combined with a rectifier to operate as a high-voltage DC power generation system for aircraft. Currently, starter/generators are used in advanced more electric aircrafts, such as the Boeing 787 and Airbus A380 [7]. The core element of starter/generators is a wound-rotor synchronous generator, and their most commonly used format is a three-stage power generation system [8–10]. The structure of a three-stage power generation system is displayed in Figure 1.

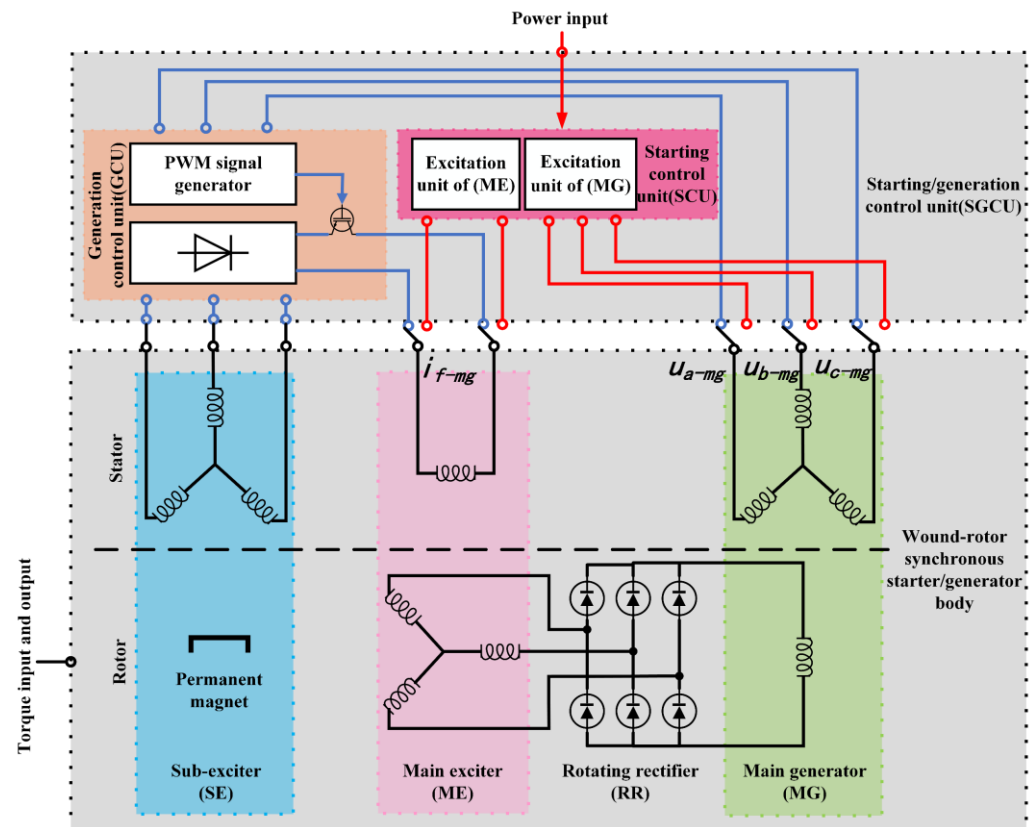


**Figure 1.** Three-stage power generation system.

As the main power source in aircraft power supply systems, WRSSG is important for safe flights and mission achievement. When the WRSSG is operating in a power generation state, it usually means that the aircraft is in flight. Therefore, it is of great significance for the research of state monitoring and fault diagnosis of WRSSG systems in this state. As shown in Figure 1, the system uses a multistage motor combined with a rotary rectifier (three-phase bridge uncontrolled rectifier circuit) to excite the main generator. The excitation mode is different from the traditional excitation mode. While completing the non-contact excitation function, it also causes a series of problems. According to the analyses of Batzel and Swanson, the two faults with the highest failure rate and the largest failure cost within this system are inter-turn short circuits of the main generator and rotating rectifier faults [11]. However, both of these faults occur on the rotating part of the system and are difficult to measure directly. Therefore, fault diagnosis and condition monitoring of the system are difficult and related research remains at the component level [12–14]. Accordingly, the establishment of a WRSSG model with high fidelity, high computational efficiency, and high versatility will be conducive to the development of digital twin technologies for the system. This will allow accurate estimates of the state quantities, which are difficult to measure in the system. Ultimately, achieving accurate fault diagnosis and state monitoring of the system will facilitate the formation of an aircraft smart grid.

Figure 1 demonstrates that the digitization tasks of this system in generating state mainly comprise nonlinear modeling of the motor, nonlinear modeling of the rotating rectifier, and the overall construction of the system. In recent years, for the modeling and analysis of motors, many studies have used finite element analysis (FEA) to solve the problem of the nonlinear relationship of motors. [15–19]. Compared to linear modeling and analysis using a traditional mathematical model, motor modeling and analysis using the FE method achieves higher fidelity [20]. Accordingly, using FE software (Version: 19.0) to build the motor body and combining ANSYS/Simplorer (Version: 19.0) and MATLAB/Simulink (Version: R2022a) software to build the external circuit is currently the main method used for power system co-simulation [21]. This method can effectively avoid errors caused by motor nonlinearities during system simulations. However, FEA is expensive in terms of both computation and time. For WRSSGs, the problem of computational cost is magnified by the presence of three motor components. The lookup table is also widely used in solving the nonlinear relationship of motors [22,23]. The method can solve the nonlinear problem in motor modeling and overcome the problem of computational cost in data collection by using the parallel computing function of FE software (Version: 19.0). However, lookup tables have strict requirements on the form of data, which is not conducive to update and supplement data. At the same time, there are also problems of interpolation and fitting. In the 1980s, intelligent algorithms such as neural networks were used to solve nonlinear problems in motors [24]. But what was established at that time was a direct connection between the input and output of the motor, which was similar to the black box model. This black box model has low interpretability and cannot analyze the relationship inside the motor. In terms of the nonlinear modeling of rotating rectifiers, Sudhoff and Wasynczuk extensively analyzed the working principle of a three-phase bridge uncontrolled rectifier circuit by adopting a rotating rectifier and established the average value model (AVM) considering the commutative process [25]. However, this model requires extensive information regarding the parameters to determine the commutation process of the three-phase bridge rectifier circuit. Moreover, the model has low compatibility with the front and back motor models and is difficult to build. A fixed-parameter AVM for three-phase bridge uncontrolled rectifier circuits has been used for frequency domain analyses of three-phase power generation systems [26,27]. However, the fixed parameter AVM cannot accurately predict the output voltage drop phenomenon caused by the commutation process in the time domain analysis of three-stage power generation systems. Owing to the commutation process, the output voltage of the rotating rectifier is lower than in the ideal state [12]. Accordingly, Jatskevich et al. proposed an AVM with variable parameters and simplified the model [28,29]. Although the model has a certain accuracy when the circuit state is stable, a lot of load parameter scanning is required before the model can be run. The effect of load parameter scanning is too dependent on the operator's experience. The WRSSG, as an important part of the power generation and starting engines of MEAs, occupies a very important position in the aviation field. At present, the main achievements still focus on frequency domain modeling and analysis [26,27]. However, the frequency domain model is less compatible with the hardware-in-the-loop platform than the time domain model. The time domain model can directly use the simulator, power amplifier, and other components to convert the calculated electrical signal into the actual electrical signal. Moreover, with traditional modeling methods, it is difficult to conduct a time domain modeling analysis of this system in the generating state. Therefore, it is necessary to introduce modern intelligent algorithms and models to enhance the interpretability of the system in the generating state.

To solve the previously mentioned problems and establish a nonlinear model with high fidelity and low computational cost with time domain analysis, this paper presents a rapidly developing intelligent algorithm and improvements of the original model to build a nonlinear model of the system in generating state. The results of this work are summarized as follows:

- A method based on FE analysis and neural network is used to solve the nonlinear relationship between current and flux in the motor.

- An improved variable parameter AVM is proposed to solve the output voltage drop and initial value problems of the rotating rectifier.
- In the time domain analysis, the d-q coordinate system is used as the reference frame to determine the signal transmission logic of the system in the power generation state. The control capability of the system is verified.

This paper contributes to the nonlinear modeling of WRSSGs in the power generation state using intelligent algorithms, improved circuit models, and the logical analysis of system signal transmission. This is conducive to the construction of a future aircraft smart grid and the application of digital twin technology in aircraft power systems. The remainder of the paper is arranged as follows: in Section 2, the working principle of the WRSSG is introduced; in Section 3, the nonlinear modeling of a motor based on the current-flux neural network is established; in Section 4, the original variable parameter AVM of the rotating rectifier is improved to reduce output voltage errors; in Section 5, the signal transmission logic of the system in the power generation state is described and the closed-loop control of the system is formed; and in Section 6, the effectiveness of each component and the whole system is verified based on RT-LAB real time simulator, and the controllability of the system model is verified by combining MIL-STD-704F with FE analysis. Finally, a summary is presented in Section 7.

## 2. Working Principle of WRSSG

Switched reluctance motors, induction motors, permanent magnet synchronous motors, and wire-wound synchronous motors can be used, in theory, as the main structure of starter/generators. Because the three-stage power generation system has been used as an aircraft power generation system for many years, the relevant technology maturity is relatively high compared to other types of motors. Therefore, the current structure of aircraft starter/generator systems is widely adopted in WRSSGs based on the three-stage power generation system. The three-stage starting/generation system's basic structure is shown in Figure 1. The system is mainly composed of a WRSSG body and a starting/generation control unit (SGCU). In the main body of the WRSSG, the sub-exciter (SE) is a permanent magnet synchronous generator; the main exciter (ME) is a rotating armature-type electric excitation synchronous motor; the main generator (MG) is an electrically excited wire-wound synchronous motor; and the rotating rectifier (RR) is a three-phase bridge uncontrolled rectifier circuit. The SGCU is the key to complete the power generation and starting engine functions of a WRSSG, which is mainly composed of a generation control unit (GCU) and starting control unit (SCU).

When the system is in the power generation state, the working principle is shown in Figure 1. The blue line in the SGCU represents the signal transmission logic of the power generation state. The aircraft engine outputs torque, which drives the rotating part of the system to rotate. The SE is excited by a permanent magnet, which generates an exciting magnetic field. The rotating shaft drives the permanent magnet to rotate, and the magnetic field rotates with the permanent magnet. Thus, the magnetic field cuts the armature winding of the SE and generates three-phase AC. The three-phase AC generated by the SE passes through the rectifier circuit and outputs DC to the field winding of the ME. An exciting field is generated in the field winding of the ME. The armature winding of the ME is located on the rotating part, which is rotated by the rotating shaft and moves relative to the exciting field generated on the ME's field winding. Therefore, three-phase AC is generated on the armature winding of the ME. The three-phase AC generated by the ME is rectified by the RR, and the DC is used for MG excitation. The magnetic field generated in the field winding of the MG rotates with the rotation of the field winding and cuts the armature winding of the MG. The three-phase AC output is generated on the armature winding of the MG, or the DC output is rectified by the rectifier circuit. The output voltage of the MG is collected by the voltage regulator and converted into PWM control signal output after processing, which is used to control the switching tube in series with the field winding of the ME. By controlling the field voltage of the ME, the output

voltage of the system can be controlled so that the output of the system can meet the power supply quality.

According to the literature [30,31], this system can also be used as a starter for starting engines. In Figure 1, the red line in the SGCU represents the signal transmission logic of the starting engine status. In the starting engine state, the SE (permanent magnet synchronous motor) part of the system does not participate in the work. The system operates as an electric motor to drive the engine to its rated speed. Initially, the system rotates at a low or zero speed. The SGCU provides an alternating current (AC) to the ME single-phase field winding, which creates a varying magnetic field in the ME air gap. At this time, the working principle of the ME is similar to that of a single-phase to three-phase transformer, and the induced voltage is generated in the rotor armature winding of the ME. Then, the RR (three-phase bridge type uncontrolled rectifier circuit) supplies power to the excitation winding of the MG. At the same time, the SGCU is used to supply a three-phase alternating current (AC) with variable frequency and variable voltage to the stator windings of the MG. At this point, the MG operates as an electric motor and the MG rotor will rotate and provide an acceleration torque and start the engine.

### 3. Motor Nonlinear Model Based on FE Analysis and Neural Network

As displayed in Figure 1, there are three motors in the WRSSG: a permanent magnet synchronous generator and two electrically excited synchronous generators. The nonlinear relationship between these motors directly affects the accuracy of the system. In the motor model, nonlinear relations (such as magnetic field saturation and spatial harmonics) are implied in the relationship between the current and the flux. In the traditional motor d-q model, the relationship between current and flux in each winding is established by using a large number of self-inductance and mutual-inductance parameters, as shown in (1).

$$\begin{aligned} d - axis : & \begin{cases} v_d(t) = \frac{d}{dt}\psi_d(t) - R_d i_d(t) - \omega \psi_q(t) \\ \psi_d(t) = -L_d(t)i_d(t) + M_{df}(t)i_f(t) \end{cases} \\ q - axis : & \begin{cases} v_q(t) = \frac{d}{dt}\psi_q(t) - R_q i_q(t) + \omega \psi_d(t) \\ \psi_q(t) = -L_q(t)i_q(t) \end{cases} \\ field : & \begin{cases} v_f(t) = \frac{d}{dt}\psi_f(t) + R_f i_f(t) \\ \psi_f(t) = -M_{fd}(t)i_d(t) + L_f(t)i_f(t) \end{cases} \end{aligned} \quad (1)$$

where  $v_d$ ,  $\psi_d$ ,  $R_d$ , and  $i_d$  are the d-axis armature voltage, flux linkage, resistance, and current, respectively. Terms  $v_q$ ,  $\psi_q$ ,  $R_q$ , and  $i_q$  are the q-axis equivalents, respectively. Terms  $v_f$ ,  $\psi_f$ ,  $R_f$ , and  $i_f$  are the field voltage, flux linkage, resistance, and current, respectively. Terms  $L_d$ ,  $L_q$ , and  $L_f$  are the d-axis, q-axis, and field inductances, respectively. Terms  $M_{df}$  and  $M_{fd}$  are the mutual inductances between the field winding and the d-axis winding, respectively, while  $\omega$  is the angular speed in electrical degrees. Equation (1) represents the voltage and flux equations of the conventional motor d-q model. The inductance parameters of the motor are constantly changing during the process from voltage building to stability. The accuracy of the motor model with fixed inductance parameters is low. The motor model with variable inductance parameters needs to establish the variation relation for each inductance parameter, which is too complicated. The motor model based on lookup table has strict requirements on the format of lookup table, which is not conducive to updating and supplementing the data. The problems of interpolation and data fitting exist simultaneously. The black box model based on neural networks directly establishes the input–output relation of motor has low explanatory ability and cannot explain the electromagnetic relation of motor. In this paper, the FE model of the motor is established based on the actual motor parameters, and then the nonlinear relation of current–flux is extracted. The current–flux neural network is trained using nonlinear current–flux data. By embedding a current–flux neural network into the improved motor d-q model, a nonlinear motor model with high fidelity, high computational efficiency, and strong interpretation is formed.

Firstly, the traditional d-q model is reformed. The reform principle is to avoid the use of differential form as much as possible and reduce the calculation cost. The inductance parameters in the flux equations are time-varying parameters that change according to the state of the motor. For high-precision motor modeling, it is necessary to establish the variation in data of each inductance parameter with respect to each current in advance. Furthermore, complete decoupling of the d- and q-axis does not happen in real situations. Therefore, the current in the d- and q-axis will also affect the flux linkage on the other winding. To use the traditional motor d-q model to complete the modeling task with high fidelity, it is necessary to introduce more mutual inductance parameters for correction. In order to solve these problems and complete the processing of nonlinear relations, the most direct way is to introduce intelligent algorithms into the model. As one of the most widely used algorithms at present, the neural network algorithm has outstanding predictive ability and computational efficiency. The single hidden layer feedforward neural network has been developed for many years and its technology is mature. In this paper, based on the conventional motor d-q model, a single hidden layer feedforward neural network is used to establish the relationship between current and flux directly. Simultaneously, the influence of the rotor position on the relationship between current and flux linkage is considered. The flux equations of the model are re-established as follows:

$$\begin{aligned}\psi_d(t) &= NNs\_d(i_d(t), i_q(t), i_f(t), \theta(t)) \\ \psi_q(t) &= NNs\_q(i_d(t), i_q(t), i_f(t), \theta(t)) \\ \psi_f(t) &= NNs\_f(i_d(t), i_q(t), i_f(t), \theta(t))\end{aligned}\quad (2)$$

where  $\theta$  is the electrical angle. The term  $NNs$  represents the corresponding current-flux linkage neural network, and (2) is the simplified flux equation set in the conventional motor d-q model. Equation (2) establishes the relationship between flux linkage and current according to rotor position. It should be noted that the complex and time-varying inductance parameters are omitted. Simultaneously, the problem that the d- and q-axis cannot be completely decoupled is solved by introducing the d- and q-axis currents into each term's flux expression. In order to obtain the nonlinear relation data of the motor, ANSYS Electronics Desktop software (Version: 19.0) was used to scan the parameters of the motor. This software (Version: 19.0) has high precision for motor modeling. This software can solve the problem of saturation of magnetic field by using functions such as customized core materials. This software can also solve the problem of spatial harmonics by using 2D or 3D structural modeling. While ensuring high precision, the software also has the function of parallel parameter scanning, which can shorten the time of parameter scanning. Here, the FEA software (Version: 19.0) (ANSYS Electronics Desktop) is used to scan the parameters of the specific motor and obtain the data describing the current-flux linkage relationship in (2). Then, the single hidden layer feedforward neural network is trained by using this data, and the current-flux linkage neural network is obtained. Compared with the traditional model, this method reduces the complexity of the flux equations. Owing to the introduction of neural networks, the model also has the ability to predict the unscanned operating points, which expands the working scope of the model. Moreover, compared with modeling the motor using FEA, the computational cost is reduced. The proposed model is as follows:

$$\begin{aligned}field &\begin{cases} \psi_f(t) = \int (v_f(t) - i_f(t)R_f)dt \\ i_f(t) = NNs\_f^{-1}(\psi_d(t), \psi_q(t), \psi_f(t), \theta(t)) \end{cases} \\ d-axis &\begin{cases} \psi_d(t) = \int (v_d(t) + i_d(t)R_d + \psi_q(t)\omega)dt \\ i_d(t) = NNs\_d^{-1}(\psi_d(t), \psi_q(t), \psi_f(t), \theta(t)) \end{cases} \\ q-axis &\begin{cases} \psi_q(t) = \int (v_q(t) + i_q(t)R_q - \psi_d(t)\omega)dt \\ i_q(t) = NNs\_q^{-1}(\psi_d(t), \psi_q(t), \psi_f(t), \theta(t)) \end{cases}\end{aligned}\quad (3)$$

Here, (3) is the nonlinear model of the motor. The model uses the FE software (Version: 19.0) to scan out the nonlinear relationship of the motor to obtain the nonlinear relationship data, and then uses the data to train the current-flux neural network, and finally the current flux neural network is embedded in the model body. The model can solve nonlinear problems such as saturation of magnetic field and space harmonic in motor. In order to verify the validity of the proposed model, the generator platform in the laboratory is used to verify the FE motor model. Then, the FE model is compared with the proposed model to verify the effectiveness of the proposed model. The generator platform is shown in Figure 2:

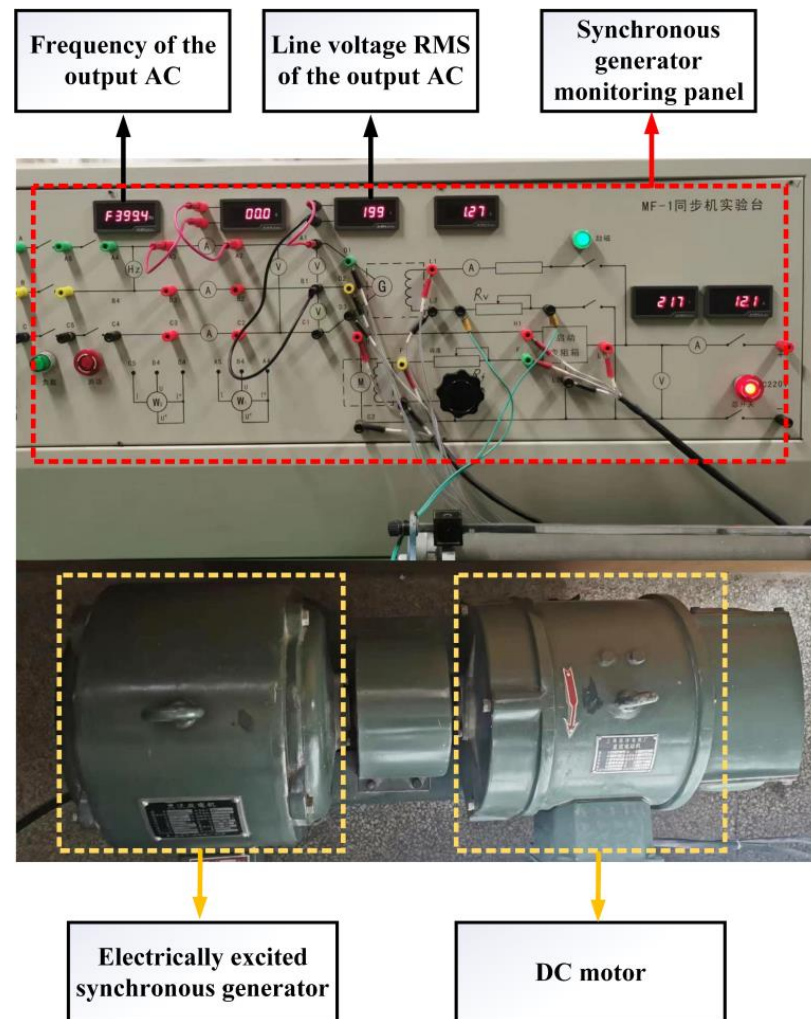


**Figure 2.** Electrically excited synchronous generator platform.

The electrically excited synchronous generator is driven by a DC motor. DC excitation is applied to the field winding of the electrically excited synchronous generator. The output voltage of the electrically excited synchronous generator is collected and displayed by the input and output display panel. Under the same input and output conditions, the output voltage comparison of the synchronous generator platform, FE model and the proposed model is shown in Figure 3.

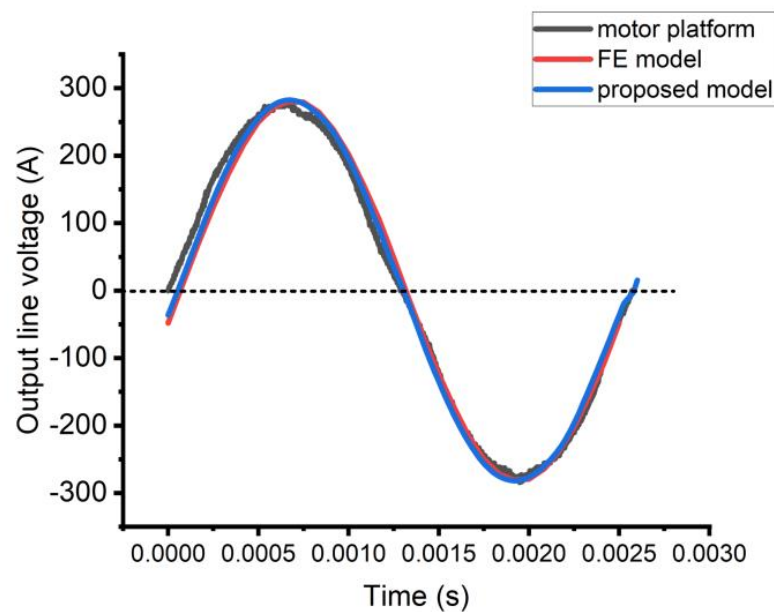


**Figure 3.** Comparison of output line voltage between synchronous generator platform and FE model.

It can be seen from Figure 3 that the FE model is highly consistent with the proposed model. Compared with the experimental platform of synchronous motor, the proposed model and FE model have high fidelity. In the first half cycle, the peak voltage of the FE motor model and the proposed model appears slightly later than that of the synchronous motor experimental platform. In the second half of the cycle, the three remained consistent. The RMS output phase voltage of the experimental platform of synchronous motor is 115 V, and the RMS output phase voltage of FE model and the proposed model is 114 V, all of which meet the output voltage standard of MIL-STD-704F.

On the basis of verifying the validity of FE model, FE analysis is used to verify the validity of the proposed model (3). At the same time, in order to verify the simulation ability of the proposed model for nonlinear relations, the paper also introduced the traditional dq linear motor model into the comparison. FE software (Version: 19.0) is used to scan the inductance parameters of the motor when the output power is 20 kVA. These inductance parameters are used in the traditional motor dq model. To make the results more straightforward, the paper not only compared the results at 20 kVA, but also compared the results at 40 kVA. In order to ensure fairness, the traditional dq model uses the inductance data obtained by FE scanning at 20 kVA, and the proposed model reduces the scanning range during FE scanning and does not scan 40 kVA working state. The AC output of the aircraft power generation system is required to meet the standard phase voltage RMS between 108 V and 118 V. In FE software (Version: 19.0), the input voltage and load of the motor are adjusted so that the output power of the motor can reach 20 kVA and 40 kVA, respectively while meeting the output voltage requirements. Then, the recorded input voltage and load conditions are applied to the proposed model and the traditional linear dq model, and the output currents of different models under different output power conditions are obtained. The relevant results are shown in Figure 4.

Figure 4 shows the output currents of these three models under different working conditions. Because the load conditions are the same, the output voltage condition is the same as the output current condition. Figure 4 shows that the proposed model maintains a high degree of consistency with FE modeling under different working conditions, which reflects the high fidelity of the proposed model. The increase in the output power of the motor requires a larger excitation current in the field winding. Under certain conditions, the increase of the excitation current will make the motor enter the state of saturation of the magnetic field. Figure 4 shows that when the output power of the motor increases from 20 kVA to 40 kVA, the gap between the output current of the traditional linear motor dq

model and the output current of the FE simulation increases significantly. This phenomenon indicates that the nonlinear (magnetic field saturation) characteristics of the motor have begun to play a role. The output results of the proposed model can still track the FE modeling results after the power increase, which shows that the proposed model has the ability to simulate the nonlinear relationship of the motor.

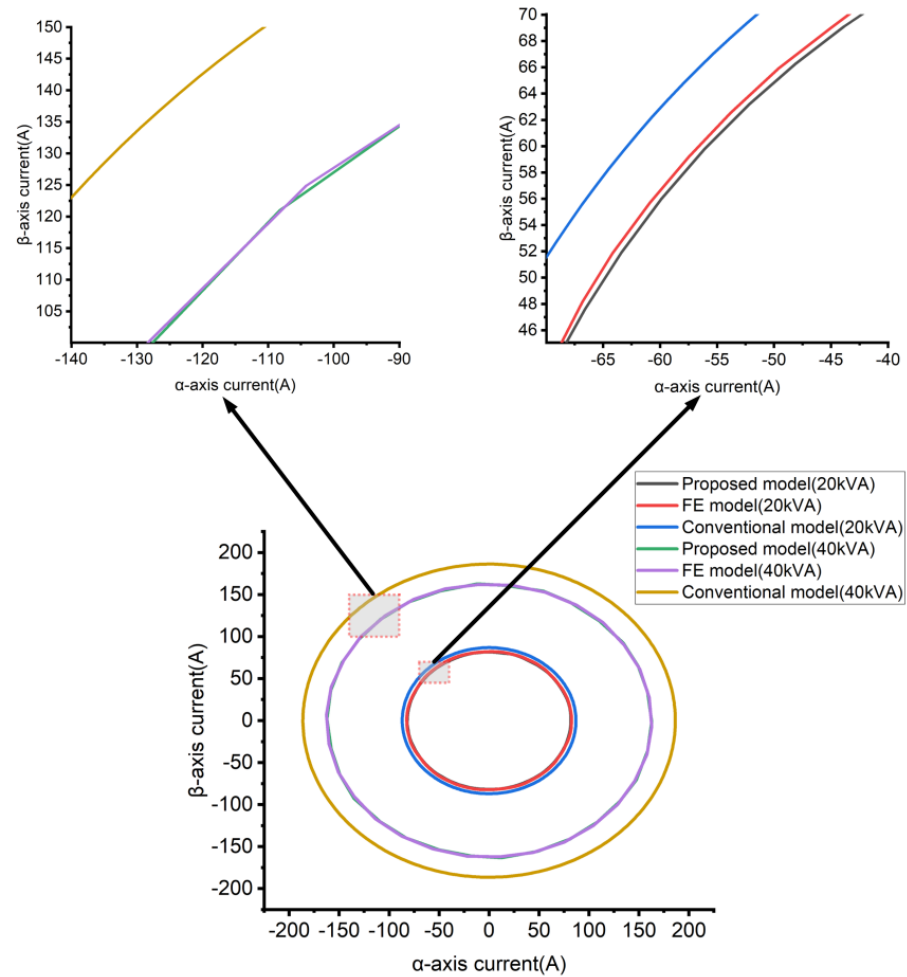


**Figure 4.** Comparison of the output current of FE model, the proposed model and the traditional dq linear model under the output power of 20 kVA and 40 kVA conditions.

In the  $\alpha\beta$  coordinate system, the current radius is taken as the index, and the relevant comparison results are shown in Table 1.

**Table 1.** The output of the proposed model is compared with that of the FE model under the output power of 20 kVA and 40 kVA conditions.

	Proposed Model	FE Analysis
Current radius of 20 kVA	81.8844 A	82.4045 A
Current radius absolute error of 20 kVA	0.5201 A	0 A
Current radius relative error of 20 kVA	0.6312%	0%
Current radius of 40 kVA	162.6027 A	162.7775 A
Current radius absolute error of 40 kVA	0.1748 A	0 A
Current radius relative error of 40 kVA	0.1074%	0%

It can be seen from Table 1 that the relative errors of the proposed model relative to the FE analysis model are all below 1%, indicating a high fidelity of the model. For simulation time comparison, this paper compares the traditional motor d-q model, the proposed model and the FE motor model. FE motor model runs in FE analysis software (Version: 19.0), traditional motor d-q linear model and proposed model run in MATLAB/Simulink (Version: R2022a). The three models use the step size of  $8.33 \times 10^{-5}$  s to calculate 1 s. The actual operation time of FE motor model is 28,609 s. The calculation efficiency of FE motor model is low and the operation cycle is long. The traditional d-q linear model and the proposed model are each run 20 times to avoid accidental phenomena because of their high computational efficiency and short computing cycle. The actual operation time of the traditional d-q model is 2.048925 s, and the actual operation time of the proposed model is 2.222805 s. These results show that the computational efficiency of the proposed model is comparable to that of the traditional d-q linear model, and much higher than that of the FE motor model. The proposed model achieves a good balance between fidelity and computational efficiency. For the FE parameter-scanning work in the proposed method, the time cost of FE parameter scanning can be reduced by using the function of parallel calculation in FE software (Version: 19.0), and the time cost is much lower than the serial calculation of FE motor model. FE parameter scanning only needs to be completed once, instead of running it from scratch multiple times like FE analysis simulations. The proposed model not only retains the nonlinear simulation capability of FE analysis, but also greatly reduces the calculation cost. This method can be used for the nonlinear modeling and analysis of WRSSGs.

The motor modeling method combining FE analysis and a neural network was used to model the three motors in a WRSSG, respectively. The relevant models are as follows:

$$\begin{cases} d-axis \\ q-axis \end{cases} \begin{cases} v_{d-se}(t) = \frac{d}{dt}\psi_{d-se}(t) - i_{d-se}(t)R_{d-se} - \psi_{q-se}(t)\omega \\ \psi_{d-se}(t) = NNS\_d(i_{d-se}(t), i_{q-se}(t), \theta(t)) \\ v_{q-se}(t) = \frac{d}{dt}\psi_{q-se}(t) - i_{q-se}(t)R_{q-se} + \psi_{d-se}(t)\omega \\ \psi_{q-se}(t) = NNS\_q(i_{d-se}(t), i_{q-se}(t), \theta(t)) \end{cases} \quad (4)$$

$$\begin{cases} field \\ d-axis \\ q-axis \end{cases} \begin{cases} \psi_{f-me}(t) = \int (v_{f-me}(t) - R_{f-me}i_{f-me}(t))dt \\ i_{f-me}(t) = NNS\_f^{-1}(\psi_{d-me}(t), \psi_{q-me}(t), \psi_{f-me}(t), \theta(t)) \\ v_{d-me}(t) = \frac{d}{dt}\psi_{d-me}(t) - i_{d-me}(t)R_{d-me} - \psi_{q-me}(t)\omega \\ \psi_{d-me}(t) = NNS\_d(i_{d-me}(t), i_{q-me}(t), i_{f-me}(t), \theta(t)) \\ v_{q-me}(t) = \frac{d}{dt}\psi_{q-me}(t) - i_{q-me}(t)R_{q-me} + \psi_{d-me}(t)\omega \\ \psi_{q-me}(t) = NNS\_q(i_{d-me}(t), i_{q-me}(t), i_{f-me}(t), \theta(t)) \end{cases} \quad (5)$$

$$\begin{cases} field \\ d-axis \\ q-axis \end{cases} \begin{cases} \psi_{f-mg}(t) = \int (v_{f-mg}(t) - i_{f-mg}(t)R_{f-mg})dt \\ i_{f-mg}(t) = NNS\_f^{-1}(\psi_{d-mg}(t), \psi_{q-mg}(t), \psi_{f-mg}(t), \theta(t)) \\ \psi_{d-mg}(t) = \int (v_{d-mg}(t) + i_{d-mg}(t)R_{d-mg} + \psi_{q-mg}(t)\omega)dt \\ i_{d-mg}(t) = NNS\_d^{-1}(\psi_{d-mg}(t), \psi_{q-mg}(t), \psi_{f-mg}(t), \theta(t)) \\ \psi_{q-mg}(t) = \int (v_{q-mg}(t) + i_{q-mg}(t)R_{q-mg} - \psi_{d-mg}(t)\omega)dt \\ i_{q-mg}(t) = NNS\_q^{-1}(\psi_{d-mg}(t), \psi_{q-mg}(t), \psi_{f-mg}(t), \theta(t)) \end{cases} \quad (6)$$

The subscript -se, -me, and -mg represent the parameters of the SE, ME and MG, respectively. In addition, (1), (2), and (3) represent the SE model, the ME model, and the MG model, respectively. Whether the voltage equation in the model adopts integral form or differential form follows the voltage dominant type mentioned in the literature [28], as shown in Figure 5:

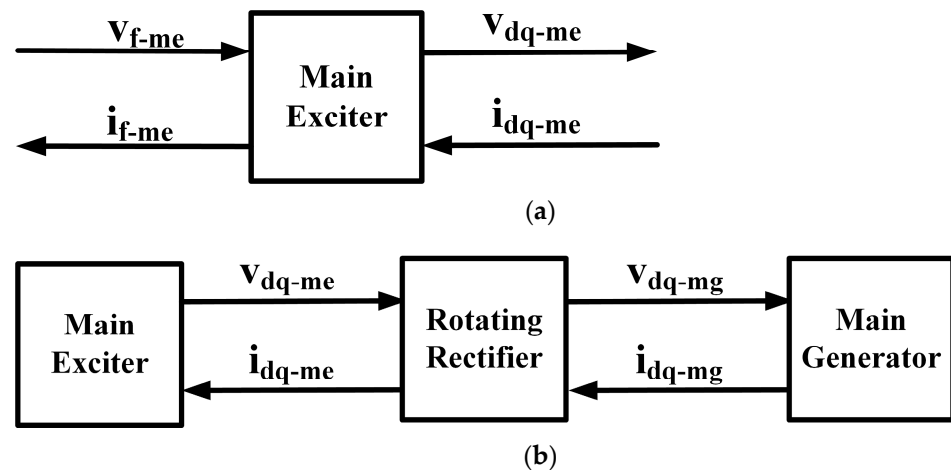


**Figure 5.** The signal transmission logic diagram of the motor. (a) ME, and (b) the connection between ME and RR.

When the motor is connected to the rectifier circuit, the relevant armature winding adopts the voltage main type (differential form), and the current is determined by the voltage and the load property. When the motor load is not a rectifier circuit, the relevant winding uses the integral form in order to reduce the calculation cost. In order to better simulate and explain the armature reaction of the motor, the voltage main type is used in the related winding. The ME is taken as an example to explain the relevant phenomena. The field current flows through the field winding of the ME to generate an excitation field, which cuts across the armature winding of the ME and generates a back electromotive force (back-EMF) on the armature winding. The armature current of the ME is determined by both the back-EMF and the load circuit. The armature current forms the armature magnetic field, which affects the original magnetic field. This is the armature reaction of the ME. Owing to the armature reaction, the flux linkage generated on each winding is iteratively updated until a new equilibrium is reached. Therefore, the voltage main type (differential form) is used in the armature winding of the SE and the ME. In the model, the single-hidden-layer feedforward neural networks with multiple input single output technology are used to fit the relationship between the current and the flux linkage (which is difficult to decouple) and the fidelity is higher than the traditional model. Equation (6) represents the MG model. To reduce the computational cost, the voltage equations are all in integral form when there are no specific requirements. Hence, the voltage equations of the MG armature winding are in an integral form. If desired, the same differential form as the ME can also be used. Given the requirements of ensuring accuracy and computational efficiency, the presented model also has strong generality and good interpretability. Although the ME and the MG are both electrically excited synchronous generators, the field winding of the ME is fixed on the stator and the armature winding is fixed on the rotor. In comparison, the form adopted by the MG is completely opposite, although the model framework adopted by both is similar. In the case of a WRSSG followed by a rectifier circuit, the model used by both is also the same. Although a large number of neural networks were used to fit the relationship between the current and flux linkage in the previous model, the effectiveness of this model is analyzed from the working principle of the motor. Since the d-q axis cannot be completely decoupled, the influence factors on each other are introduced into the d-q axis current-flux linkage relationship. Moreover, in the process of establishing the SE model, the flux generated by the permanent magnet and by the d-axis current is integrated into the d-axis flux, ensuring the model has high fidelity. The single-hidden-layer feed-forward neural network is only used for fitting the relationship between the current and the flux linkage. Therefore, the interpretability of the model is maintained at a high level under the condition of ensuring the model's high fidelity.

#### 4. Improved Variable Parameter AVM

As the connection circuit between the motors, the RR directly determines the performance of the WRSSG. The RR uses a three-phase bridge uncontrolled rectifier circuit (Figure 6) and is installed on the rotating shaft with high-speed rotation.

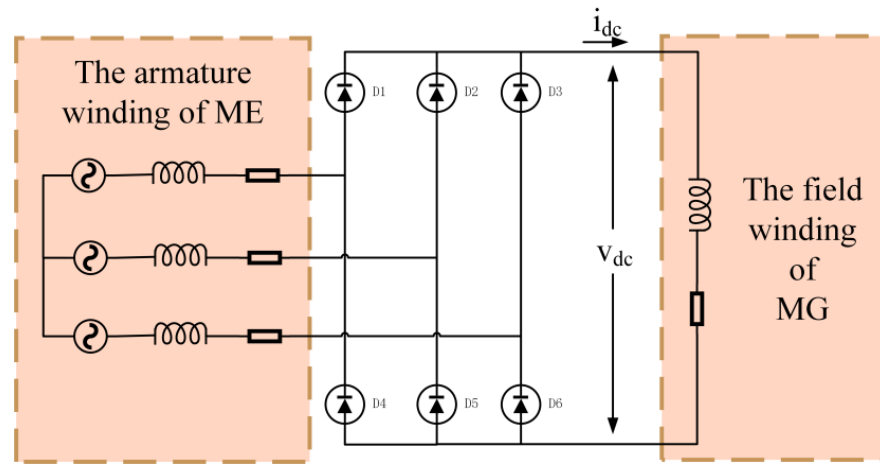


Figure 6. The three-phase bridge uncontrolled rectifier circuit.

For the condition monitoring and fault diagnosis of the WRSSG, condition monitoring of the RR is one of the emphases. In the literature [25,26], based on an analysis of the working state of the three-phase bridge uncontrolled rectifier circuit [24], researchers have used the AVM with fixed parameters to complete its modeling to achieve certain results in the frequency domain analysis. The AVM with fixed parameters is as follows:

$$\begin{aligned}
 v_{dc}(t) &= \frac{3\sqrt{3}}{\pi} (v_{d-me}(t) \sin \delta(t) + v_{q-me}(t) \cos \delta(t)) \\
 i_{d-me}(t) &= \frac{2\sqrt{3}}{\pi} i_{dc}(t) \sin(\delta(t) + \zeta) \\
 i_{q-me}(t) &= \frac{2\sqrt{3}}{\pi} i_{dc}(t) \cos(\delta(t) + \zeta) \\
 \delta(t) &= \arctan \frac{v_{d-me}(t)}{v_{q-me}(t)}
 \end{aligned} \tag{7}$$

where  $v_{dc}$  and  $i_{dc}$  are the output voltage and current of the RR, respectively. Terms  $v_{d-me}$ ,  $v_{q-me}$ ,  $i_{d-me}$ , and  $i_{q-me}$  are the armature voltages and currents of the ME under the d-q frame. Term  $\delta$  is the power angle of the ME and  $\zeta$  is the angle of the armature current behind the armature voltage of the ME. There is a fixed ratio relationship between the input and output electrical signals in an AVM with fixed parameters. From Figure 6, it is evident that both the input and output terminals are connected to the motor winding. These windings are all perceptual. Therefore, in the process of commutation of the rectifier circuit, there will be a commutation delay in the circuit, which will cause an output voltage drop. The output voltage of a real RR will be lower than the AVM output with fixed parameters when the WRSSG works stably. Moreover, the commutation delay of the three-phase bridge uncontrolled rectifier circuit depends on the circuit properties of the input and output. Therefore, the fixed parameter AVM cannot achieve good results in the time domain analysis, regardless of how the parameters are adjusted. Hence, it is necessary to introduce the circuit properties of the input and output terminals into the analysis of the three-phase bridge uncontrolled rectifier circuit to obtain improved time domain analysis results.

In [28,29], the researchers introduced the circuit properties of the input and output terminals into the AVM and established the variable parameter AVM, as follows:

$$\begin{aligned}
 \text{body : } & \left\{ \begin{aligned} \bar{v}_{qs}^r(t) &= \alpha(t) * \bar{v}_f(t) * \cos(\delta_r(t)) \\ \bar{v}_{ds}^r(t) &= \alpha(t) * \bar{v}_f(t) * \sin(\delta_r(t)) \\ \bar{i}_{dc}(t) &= \beta(t) * \sqrt{(\bar{i}_{ds}^r(t))^2 + (\bar{i}_{qs}^r(t))^2} \\ \delta_r(t) &= \arctan\left(\frac{\bar{v}_{ds}^r(t)}{\bar{v}_{qs}^r(t)}\right) = \arctan\left(\frac{\bar{i}_{ds}^r(t)}{\bar{i}_{qs}^r(t)}\right) - \varphi(t) \end{aligned} \right\} \\
 \text{scanning parameter : } & \left\{ Z = \frac{\bar{v}_f(t)}{\sqrt{(\bar{i}_{ds}^r(t))^2 + (\bar{i}_{qs}^r(t))^2}} \right\} , \\
 \text{updated parameters : } & \left\{ \begin{aligned} \alpha(t) &= \frac{\sqrt{(\bar{v}_{ds}^r(t))^2 + (\bar{v}_{qs}^r(t))^2}}{\bar{v}_f(t)} \\ \beta(t) &= \frac{\bar{i}_f(t)}{\sqrt{(\bar{i}_{ds}^r(t))^2 + (\bar{i}_{qs}^r(t))^2}} \\ \varphi(t) &= \arctan\left(\frac{\bar{i}_{ds}^r(t)}{\bar{i}_{qs}^r(t)}\right) - \arctan\left(\frac{\bar{v}_{ds}^r(t)}{\bar{v}_{qs}^r(t)}\right) \end{aligned} \right\} \tag{8}
 \end{aligned}$$

$$\bar{f} = \frac{1}{T_{SW}} \int_{t-T_{SW}}^t f(t) dt. \tag{9}$$

All electrical parameters in (8) are averaged in the output period of the three-phase bridge rectifier circuit by Formula (9). For a 1000 Hz AC input,  $T_{SW}$  is 1/1000/6 s. The circuit model (8) is in d-q coordinate system. The three-phase AC at the input is projected from the abc coordinate system to the d-q coordinate system. In (8),  $\bar{v}_{qs}^r(t)$ ,  $\bar{v}_{ds}^r(t)$ ,  $\bar{i}_{qs}^r(t)$ , and  $\bar{i}_{ds}^r(t)$  represent the q-axis voltage component, d-axis voltage component, q-axis current component, and d-axis current component of the input three-phase AC in the d-q coordinate system, respectively.  $\bar{v}_f(t)$  and  $\bar{i}_f(t)$  represent the output voltage and output current of the three-phase bridge rectifier circuit.  $Z$  represents the parameters that the model needs to scan, as determined by the nature of the load.  $\alpha(t)$  and  $\beta(t)$  represent the input/output ratio of the three-phase bridge rectifier circuit.  $\varphi(t)$  indicates the angle of the input current lagging voltage, which is determined by the nature of the load. The AVM of variable parameters works as follows: first, adjust the  $Z$  value by changing the nature of the output load, and scan out the corresponding  $\alpha(t)$ ,  $\beta(t)$ , and  $\varphi(t)$  values while adjusting the  $Z$  value, and establish the lookup table. When the model is running, the  $Z$  value is calculated, and the corresponding variable ratio is obtained by looking up the table, and the system state is solved by the variable ratio. The process of parameter scanning exists in this method. The task of parameter scanning is large, the target is not clear, and the nature of load seriously affects the simulation results. Therefore, according to the load properties of the RR, this paper proposes an improved AVM model of the variable parameter, which is as follows:

$$\begin{aligned}
 \text{model body : } & \left\{ \begin{aligned} \bar{v}_{f1}(t) &= \bar{v}_{f2}(t) + L_{leakage} \frac{d\bar{i}_f(t)}{dt} \\ \bar{v}_{qds}(t) &= \bar{v}_{qs}^r(t) \cos(\delta_r(t)) + \bar{v}_{ds}^r(t) \sin(\delta_r(t)) \\ \bar{v}_{f1}(t) &= \frac{\bar{v}_{qds}(t)}{\alpha(t)} \\ \bar{i}_{qs}^r(t) &= \bar{i}_{qds}^r(t) \cos(\delta_r(t) + \varphi(t)) \\ \bar{i}_{ds}^r(t) &= \bar{i}_{qds}^r(t) \sin(\delta_r(t) + \varphi(t)) \\ \|\bar{i}_{qds}\| &= \frac{\bar{i}_f(t)}{\beta(t)} \\ \delta_r(t) &= \arctan\left(\frac{\bar{v}_{ds}^r(t)}{\bar{v}_{qs}^r(t)}\right) \\ \varphi(t) &= \arctan\left(\frac{\bar{i}_{ds}^r(t)}{\bar{i}_{qs}^r(t)}\right) - \arctan\left(\frac{\bar{v}_{ds}^r(t)}{\bar{v}_{qs}^r(t)}\right) \end{aligned} \right\} \tag{10} \\
 \text{updated parameters : } & \left\{ \begin{aligned} \alpha(t) &= \frac{\|\bar{v}_{qds}(t_1)\|}{\bar{v}_{f1}(t_1)} \\ \beta(t) &= \frac{\bar{i}_f(t_1)}{\|\bar{i}_{qds}(t_1)\|} \end{aligned} \right\}
 \end{aligned}$$

Figure 7 shows the specific form of the MG field winding. In (10), variable parameters such as  $\bar{v}_{f1}(t)$ ,  $\bar{v}_{f2}(t)$ ,  $\bar{i}_f(t)$ , and  $L_{leakage}$  are introduced according to the specific form of the MG field winding after the RR, and the leakage inductance on the MG field winding is considered to better establish the output circuit of the RR. On the basis of the variable parameter AVM, hysteresis is introduced to avoid the parameter scanning before the model is established, and  $t_1$  represents the state of the system at the previous time. The initial values of  $\alpha(t)$  and  $\beta(t)$  are  $\frac{\pi}{3\sqrt{3}}$  and  $\frac{\pi}{2\sqrt{3}}$  respectively. It can be seen from (10) that the model completes the prediction of the output voltage drop phenomenon of the RR by introducing the property of the specific circuit and the real-time calculation of the variable parameters  $\alpha$  and  $\beta$ . The solution logic of the model is as follows: first, the initial values of  $\alpha$  and  $\beta$  and the specific properties of the circuit are used to drive the model ontology calculation, and the model ontology calculates the current state of the RR, and then uses the state of the RR to update the variable parameters  $\alpha$  and  $\beta$ , and finally uses the updated variable parameters to update the state of the model. This model not only retains the advantages of the variable parameter average value model to accurately predict the output voltage drop phenomenon, but also avoids the work of parameter scanning before modeling, which has high fidelity and high computational efficiency.

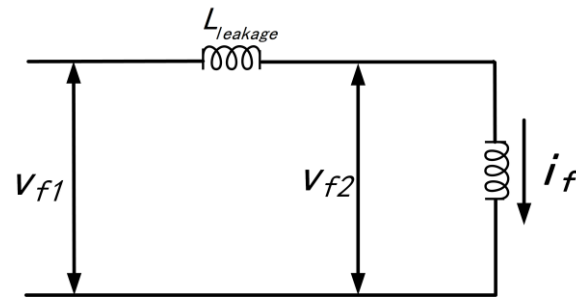


Figure 7. Load end of RR.

## 5. Whole System Modeling and Signal Transmission Logic Analysis

The overall modeling and signal transmission logic analysis of the WRSSG in the generating state involves two main aspects:

- Nonlinear modeling and analysis of the controller;
- Signal transmission logic analysis of the whole system.

In Sections 3 and 4, the signal transmission logic between the motor and the rectifier circuit was shown in Figure 5. This section mainly focuses on the nonlinear modeling of the controller and its combination with other parts. The WRSSG in its generating state is a closed-loop and is regulated by a controller, which determines the power supply quality of the system. In the power generation state, the working principle of the controller is as follows: first, the output phase voltage of the MG is measured and the three channel voltage signals are averaged after taking the RMS value. Then, the voltage deviation is obtained by comparing it with the reference voltage. This deviation signal is then input to the PWM signal generator after passing through the PI controller. The switch tube, which is connected in-series with the field winding of the ME, is controlled by the PWM Signal. The whole system is regulated by controlling the field voltage on the field winding of the ME to ensure that the output of the system meets aviation standards MIL-STD-704F. According to the working principle of the controller, the logic diagram of the whole system signal transmission displayed in Figure 8 is established.

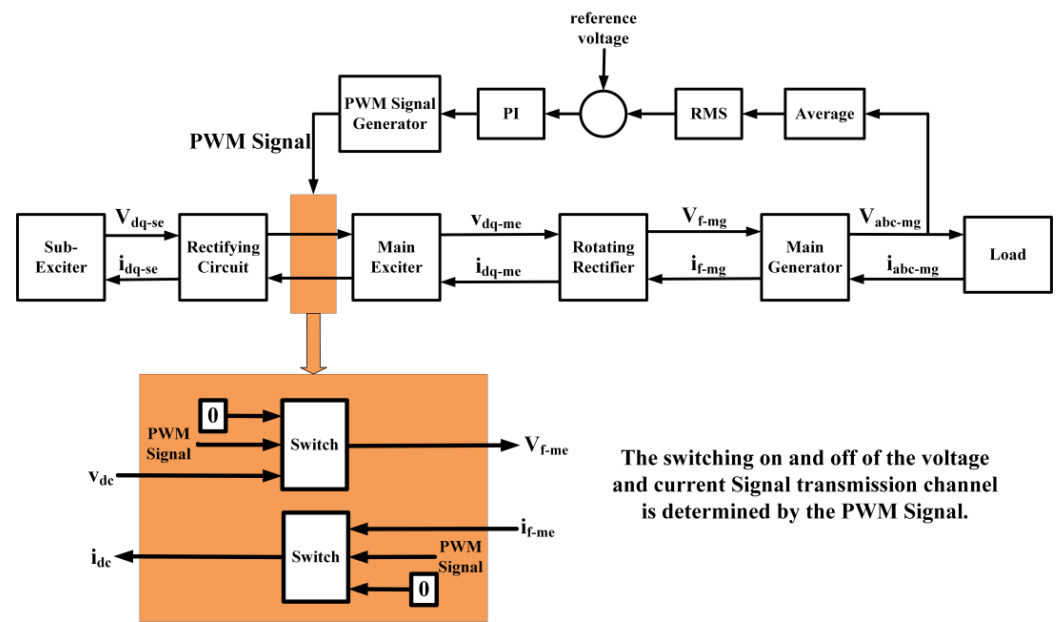


**Figure 8.** Signal transmission logic of WRSSG in generating state.

When the controller is regulating the voltage on the field winding of the ME, to avoid any impact on the circuit caused by sudden increases and decreases in current, the WRSSG has a freewheeling diode in the field winding of the ME in reverse parallel connection. This freewheeling diode ensures continuity of the current in the field winding and protects the circuit. However, due to the existence of the freewheeling diode, the current and voltage before and after the switch are inconsistent. Moreover, this introduces a new nonlinear relationship into the system, which increases the difficulty of system modeling. The specific circuit structure is displayed in Figure 9.

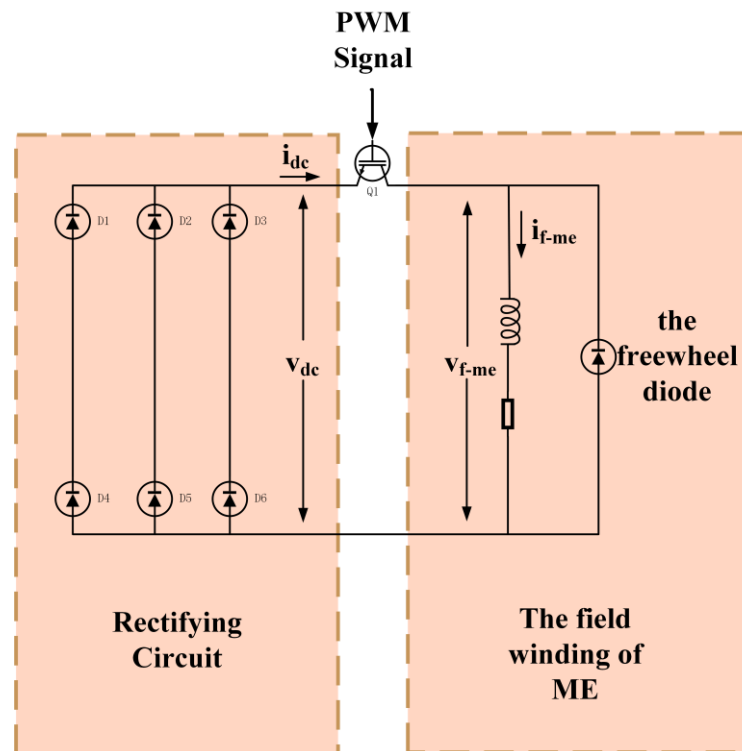


**Figure 9.** Connection circuit between rectifier circuit and ME.

The ME involved in Figure 9 is a rotating armature type synchronous generator. The switching tube controlled by PWM signal is in series with the ME's field winding and is located on the stator side of the system. This switching tube, controlled by PWM signal, controls the electrical signal input to the ME field winding. However, the freewheeling diode counter-parallel on the field winding makes the voltage and current before and after the switch tube inconsistent. To solve these problems, this paper highlights the analysis of the actual circuit and introduces two virtual control switches as shown in Figure 8. The actual circuit is shown in Figure 9, and the position of the virtual switch is visible in Figure 8. When the PWM signal control switch tube is disconnected, the output voltage of the rectifier circuit cannot be transferred to the ME's field winding, but in order to protect the winding and avoid excessive current change on the winding, the reverse parallel diode is introduced in actual circuit. The presence of the anti-parallel diode makes the field current still exist in the field winding, but the disconnection of the switching tube makes the current signal not transmitted to the rectifier circuit. When the PWM signal control switch tube is switched on, the rectifier circuit outputs voltage to the ME's field winding, and the output current of the rectifier circuit is consistent with the ME's field current. At this time, the freewheeling diode does not function. Based on the above analysis, this paper introduces two virtual switches into the model, as shown in Figure 8. The virtual switch is controlled by PWM signal to solve the problem of inconsistent electrical signals in front and back circuits. Furthermore, the controller regulates the field voltage on the field winding of the ME according to the three-phase AC output of the MG to realize closed-loop control of the system in the generating state.

The overall modeling logic of the WRSSG in the generating state mainly relies on the connection logic of the motor and the rectifier circuit. Each motor stage is excited by the voltage output of the rectifier circuit connected to the front end or the permanent magnet, which generates the EMF on the armature winding and outputs to the rectifier circuit (or load circuit) connected to the back end. The properties of the EMF and the back-end connection circuit determine the armature current on the armature winding, which generates the armature magnetic field. Together, the armature and field magnetic fields determine the EMF generated on each winding. In this paper, park transform and inverse park transform are used to connect different kinds of loads on the load side of the MG model. After continuous iteration, the system reaches equilibrium. By measuring the output of the system, the controller uses the switch tube to control the field voltage applied on the field winding of the ME to achieve closed-loop control of the system in generating state. According to the motor nonlinear modeling conducted in Section 3, the improved variable parameter AVM in Section 4, and the whole system signal transmission logic in Figure 8, the nonlinear modeling of the WRSSG in the generating state is completed.

## 6. Validation and Analysis of the Model Based on the RT-LAB Real-Time Simulator

The validity verification and analysis of the model are divided into two parts: fidelity and control ability. In the validation and analysis of the system, MIL-STD-704F aviation standard is used in this paper. The specific requirements of the standard are as follows:

Table 2 shows the power supply quality requirements for aircraft power generation systems. For the aircraft power generation system, it is mainly to control the output AC of the MG to meet the corresponding quality requirements. The requirements in Table 2 are for the MG output voltage. Based on MIL-STD-704F, the effectiveness and control ability of the proposed model are verified and analyzed in this paper.

**Table 2.** The MIL-STD-704F aviation standard.

Parameter	Limits
Steady-state voltage	108.0 to 118.0 V RMS
Voltage unbalance	3.0 V
Voltage modulation	2.5 V RMS maximum
Voltage phase difference	116° to 124°
Distortion factor	0.05 maximum
Crest factor	1.31 to 1.51
DC component	+0.10 to −0.10 V
Steady-state frequency	393 Hz to 407 Hz
Frequency modulation	4 Hz
Peak characteristics	±271.8 V

In this paper, the RT-LAB real-time simulator is used to verify and analysis the WRSSG nonlinear model.

### 6.1. Implementation of WRSSG Nonlinear Model Based on RT-LAB Real Time Simulator

The application of hardware-in-the-loop technology can solve the problems of high cost and long cycle of current product development, and hardware-in-the-loop technology is the most effective and feasible way to study irreversible and uncontrollable faults. The successful compilation of nonlinear models in real-time simulators is a necessary step toward build hardware-in-the-loop platforms. For aircraft WRSSGs in the generating state, the fault diagnosis and condition monitoring of the system directly determine the working state of the aircraft and affects the generation of combat effectiveness. The RR and the MG field winding are the two parts with the highest failure rate and the highest failure cost. Because they are located on the rotating shaft driven by the engine, the electrical parameters related to their state cannot be measured directly. When the electrical parameters of other positions are used, the state information that can reflect the above faults will be blurred due to the influence of nonlinear factors in the signal transmission process. Therefore, research of system condition monitoring and fault diagnosis has been slow. The establishment of a hardware-in-the-loop test platforms for aircraft WRSSGs can make use of digital twins, intelligent algorithms, and other technologies to study the status monitoring and fault diagnosis of aircraft power generation system, which is more conducive to the study of system fault mechanism. Studies at the system level can also analyze the fault transmission and coupling mechanism. Fault diagnosis and condition monitoring of WRSSGs in the generating state are analyzed at the system level.

In this paper, an RT-LAB real-time digital simulation platform is used to verify the nonlinear model of the system. It is a scientific instrument for power and electrical engineering fields, which can be seamlessly integrated with a MATLAB/Simulink (Version: R2007a) to achieve real-time interactions between Simulink models and real environments.

Figure 10 shows the basic structure of the WRSSG validation platform. In this paper, the nonlinear model of an WRSSG in the generating state is reconstructed according to the compiling rules of RT-LAB. In order to make better use of the performance of the machine, the system is divided into seven parts (SE, rectifier circuit, ME, RR, MG, SGCU, and human–computer interaction). Each part transmits signals through the OpComm module. Apart from the human–computer interaction part, which is in the upper computer, the rest of the parts are respectively called a core in the RT-LAB machine for calculation, so that the calculation force can meet the requirements of the nonlinear model. The whole operation is carried out in the MATLAB/Simulink (Version: R2007a) environment. During the test, a fixed step solver is used. The calculation step is 50 microseconds, which takes into account the output voltage frequency of the WRSSG, and also ensures that the test platform can complete the calculation task of the specified time. The duration is permanent and the system is stopped manually by the operator. The execution of the nonlinear model meets our expectations, and there is no time-out throughout the whole process.

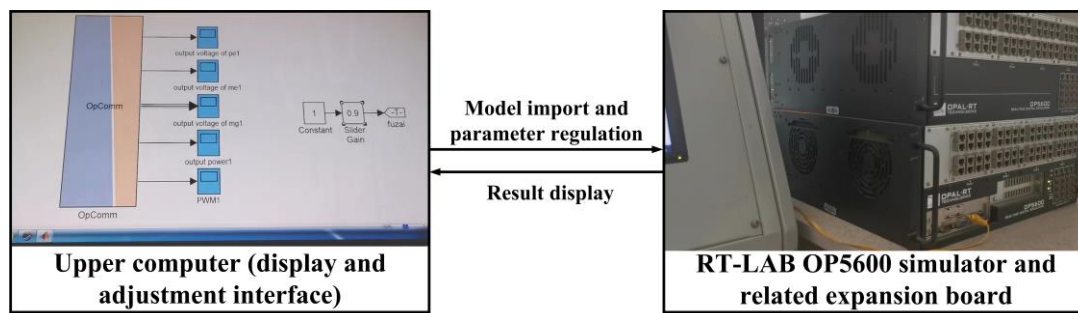


**Figure 10.** The WRSSG verification platform based on RT-LAB real time simulator.

### 6.2. Fidelity Verification and Analysis

In order to verify the validity of the nonlinear model and the accuracy of the theory, the results of the FEA were compared with those of the real time simulator. Herein, actual WRSSG parameters provided by the plant were used to establish the dynamic model in the commercial FEA software (Version: 19.0) (ANSYS Electronics Desktop). Combined with the FEA, the proposed WRSSG model was verified. The verification results of the motor in the WRSSG are as follows:

Figure 11 shows the output voltage waveforms of different motors under different working conditions by means of global and local coordination. Figure 11 shows the state changes of the whole process of the component using the global diagram and the relevant details using the local enlarged diagram. The same representation method is used in the subsequent correlation result figure. Figure 11 demonstrates that the three motor parts in the established nonlinear model of the WRSSG in generating state achieved high fidelity when the system worked as a closed loop. During  $[0 \text{ s}, T]$ , the system output voltage was less than the rated voltage and the voltage regulator did not operate. At  $[T, 0.1 \text{ s}]$ , the output voltage of the system approached the rated output voltage and the voltage regulator started to stabilize the output voltage of the system near the rated voltage. Figure 11a displays the output result of the SE in the system, from which it is evident that the output voltage of the proposed SE model had high phase and amplitude fidelity in both the voltage-building and normal operation processes. Moreover, it successfully predicted the change trend and degree of the output of the SE. Figure 11b represents the output result of the ME in the system, from which it is evident that the proposed nonlinear model of the ME had high fidelity in terms of both the voltage-building and the normal working state. Figure 11c demonstrates that the output phase voltage of the proposed nonlinear model of the MG was slightly larger than that of FEA during the process of voltage building. After the voltage regulator started working, the proposed model achieved high fidelity and could accurately predict the amplitude and phase of the voltage.

When the switch tube on the field winding of the ME started to be controlled on and off, the whole system was affected accordingly. Among them, the armature winding of the SE was connected to the field winding of the ME through the rectifier circuit. When the switch tube was disconnected, the current in the armature winding of the SE was cut off and the armature reaction that was originally present in the SE disappeared. The armature winding of the SE was inductive. In normal operation, the current lagged the voltage and the armature reaction was demagnetization. When the switch tube was disconnected, the armature reaction disappeared and the output voltage of the SE increased accordingly, as demonstrated in Figure 11a. When the switch tube was disconnected, the field voltage input to the ME suddenly reduced to zero. However, because the field winding of the ME was anti-parallel to the freeform diode, the current on the field winding of the ME exhibited a continuous (not abrupt) change. Therefore, the output voltage of the ME fluctuated under the action of the controller to regulate the output of the system near the rated voltage. Finally, the output voltage of the MG was stable around the rated voltage and met the requirements of the standard.

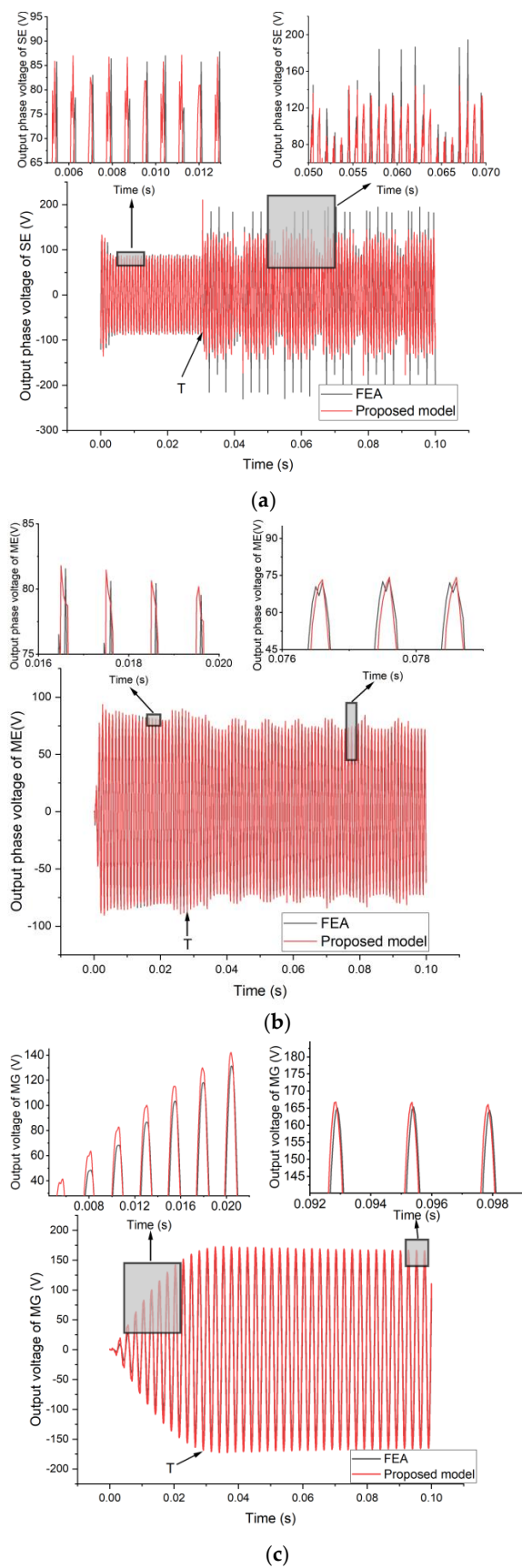
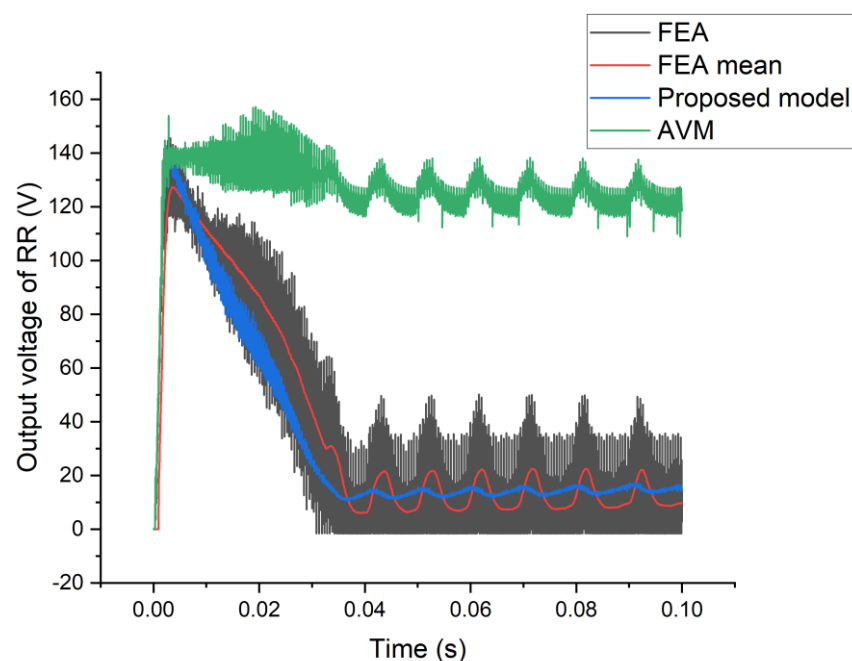


Figure 11. Motor output phase voltage waveforms: (a) SE, (b) ME, and (c) MG.

Several models of RR proposed in Section 4 were verified and compared, as displayed in Figure 12. From the figure, it is evident that the output voltage of the RR significantly reduced due to the existence of the commutation process after the voltage construction of the ME was completed, accompanied by voltage fluctuations. When the controller started working, the output voltage fluctuated significantly around 15 V. To observe the working state of the RR more intuitively, the output voltage was averaged at a frequency of 1000 Hz. The specific phenomenon is depicted in Figure 12. The AVM with fixed parameters could complete the simulation of RR more effectively during the process of voltage building. However, when the RR was working stably, due to neglecting the voltage drop in the commutation process, the fixed parameter AVM did not exhibit the voltage drop phenomenon after the voltage building was completed and maintained a large voltage output. Even when the controller was working, the output voltage of this model only fluctuated slightly. The output voltage of the fixed parameter AVM was much higher than the output voltage of the analog circuit built by software when the system was working stably. However, this error is not acceptable in the time domain analysis of a WRSSG in the generating state. The improved variable parameter AVM proposed in Section 4 achieved high fidelity in both the voltage-building and stabilization processes. The improved variable parameter AVM accurately predicted the time when output voltage sag occurred and the amplitude of the voltage sag when the system was stable. Accordingly, compared with the fixed parameter AVM, the improved variable parameter AVM would be more suitable for the modeling and analysis of a WRSSG in the time domain.



**Figure 12.** Comparison of output voltage of RR.

### 6.3. Control Capability Verification and Analysis

The voltage regulation capability of the WRSSG is the key factor that determines the power supply quality of an aircraft power generation system. In this paper, the control ability of the system was verified according to MIL-STD-704F.

Figure 13 reflects the working state of the system when the output power was 40 kW. The system started to trigger the controller for voltage regulation at  $T_1 = 0.04$  s. Before  $T_1$ , since the RMS value of the system output phase voltage was much lower than the rated voltage, the controller regulated the switch tube in the normally open state. After  $T_1$ , as the output phase voltage gradually increased, the controller regulated the duty ratio of the switch tube to decrease the voltage accordingly. Under the action of the controller, the RMS value of the output phase voltage of the system was 114.10 V, which was within the rated

voltage range. Combined with MIL-STD-704F, the system was tested in more detail, and the test results are presented in Table 3.

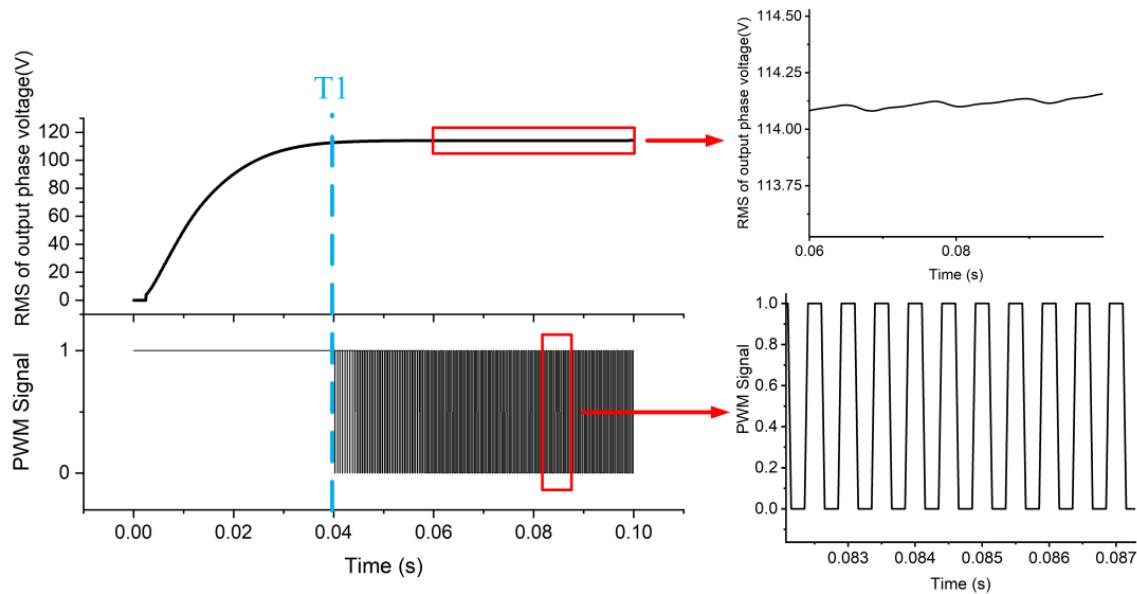


**Figure 13.** RMS value of output phase voltage and PWM control signal during normal operation of the system.

**Table 3.** Verification of steady-state characteristics and transient characteristics based on MIL-STD-704F.

Parameter	Proposed Model	Limits
Steady-state voltage	113.931 V	108.0 to 118.0 V RMS
Voltage unbalance	0.0558 V	3.0 V
Voltage modulation	0.0566 V	2.5 V RMS maximum
Voltage phase difference	120.24°	116° to 124°
Distortion factor	0.0081	0.05 maximum
Crest factor	1.41	1.31 to 1.51
DC component	$-4.2372 \times 10^{-4}$ V	+0.10 to -0.10 V
Steady-state frequency	400 Hz	393 Hz to 407 Hz
Frequency modulation	0 Hz	4 Hz
Peak characteristics	161.0 V	$\pm 271.8$ V

As displayed in Table 3, the system was tested in both steady and transient states. The state of the system after the stable output was used in the analysis with a time range of [0.06 s, 0.10 s]. From Table 3, it is evident that the output voltage of the system met the MIL-STD-704F standard in all aspects. Since the output of the system was connected to a balanced three-phase load, the voltage unbalance was significantly below the maximum upper limit of 3.0 V. During the test process, the load was constant and the voltage modulation and other parameters also met the requirements. Combined with the appeal analysis, it was evident that the nonlinear model of the WRSSG established in this paper met the parameter requirements of the MIL-STD-704F. It is clear that changes in load would test the system's voltage regulation and control capabilities. Accordingly, to further test the control ability of the analytical model, the nonlinear model was tested for sudden load increases and decreases, and the test results are displayed in Figures 14 and 15.

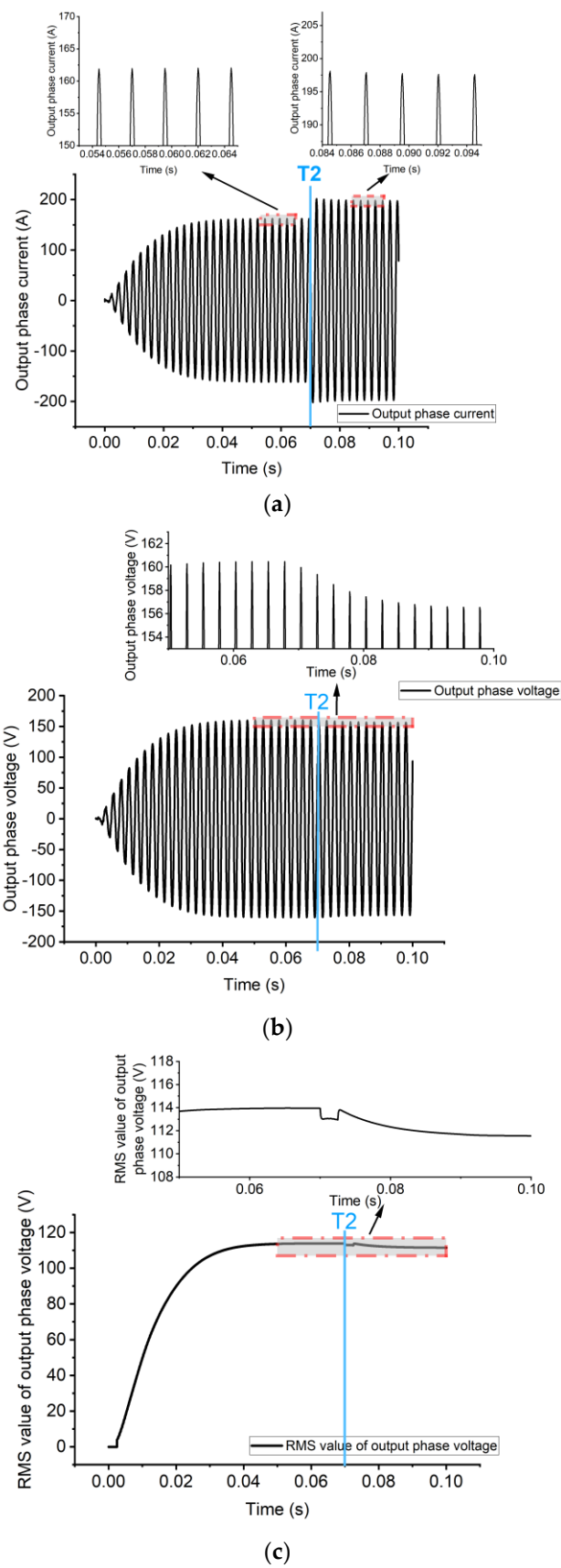
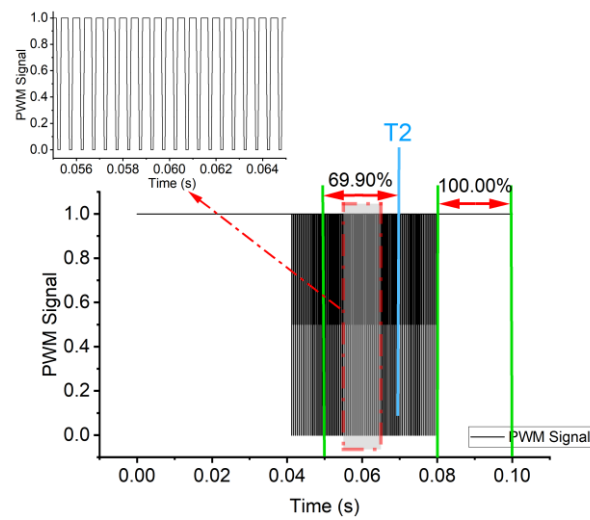
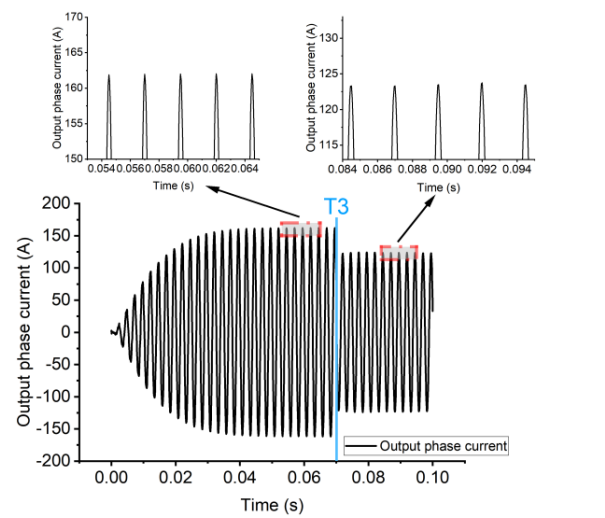


Figure 14. Cont.

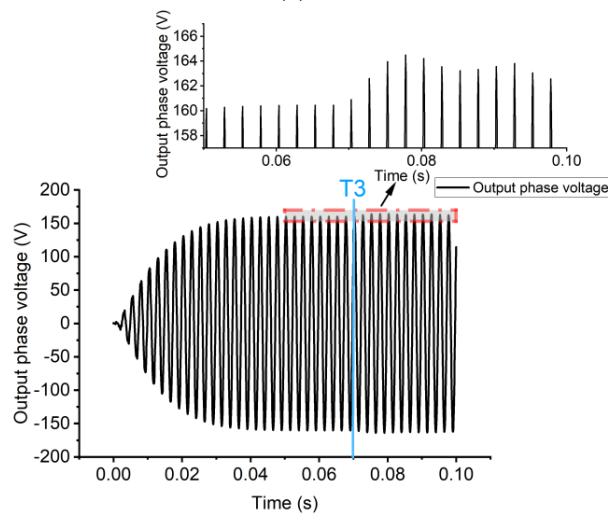


(d)

**Figure 14.** The system output power increases from 40 kW to 50 kW. (a) Output phase current, (b) output phase voltage, (c) RMS value of output phase voltage, and (d) PWM control signal.

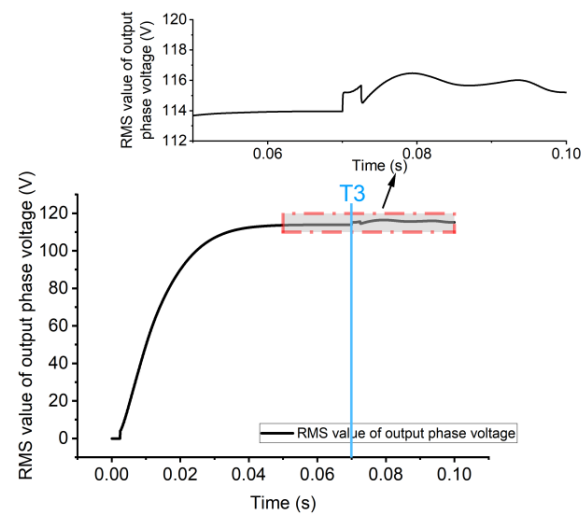


(a)

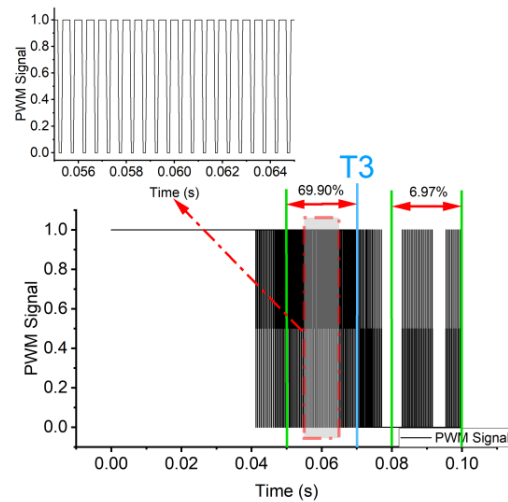


(b)

**Figure 15.** Cont.



(c)



(d)

**Figure 15.** The system output power decreases from 40 kW to 30 kW. (a) Output phase current, (b) output phase voltage, (c) RMS value of output phase voltage, and (d) PWM control signal.

Figure 14 reflects the state change of the system when the output power increased abruptly from 40 to 50 kW. At time point T2, the system output power suddenly increased and the output phase current increased accordingly. To regulate the output voltage within the rated voltage range, the controller increased the duty ratio of the switch tube and enhanced the excitation phenomenon of the ME. The output phase voltage remained almost constant under the action of the controller. Owing to the output phase voltage RMS fluctuations, there was a slight decline in the RMS output voltage. However, the output voltage remained within the rated voltage range, meeting the supply quality standard. At [0.08 s, 0.10 s], the duty cycle of the PWM signal increased from 69.60% to 100.00%. This phenomenon indicated that the generation capacity of the system had been reached. Under this set of parameters, the maximum generation power of the WRSSG was 50 kW. Figure 15 reflects the state change of the system when the output power suddenly reduced from 40 to 30 kW. Contrary to the case of the output power surge, the system reduced the field current on the field winding of the ME by reducing the duty ratio of the switch tube from 69.90% to 6.97% to control the output voltage of the system within the rated voltage range. The graph of the output phase voltage indicates that the system had strong control capabilities and could be stabilized within the range specified by the standard.

The results above show that the proposed model performs well in RT-LAB real time simulator, and the nonlinear model can be used in the state monitoring and fault diagnosis of aircraft power system.

## 7. Conclusions

In aircrafts with WRSSGs, the nonlinear relationship of the power system in generating state mainly originates from the internal structure of the power generation system and the external load. In this paper, the nonlinear relationships from the internal power generation system were analyzed. In the motor, the nonlinear relationship mainly existed in the relationship between the current and the flux linkage. Nonlinear factors (such as magnetic field saturation and space harmonics) were included in the relationship between the current and the flux linkage. The use of FE analysis and neural networks accurately completed the nonlinear modeling of the motor and solved the nonlinear problem of the current and the flux linkage. The advantages of the proposed model (high fidelity, high computational efficiency and strong interpretability) are verified by combining the synchronous generator platform and FE analysis software (Version: 19.0). In the RR part, the nonlinear relationship mainly originated from the voltage drop phenomenon during the commutation process of the circuit. The improved variable parameter AVM proposed in this paper accurately predicted the voltage drop phenomenon caused by the commutation process and achieved an accurate prediction of the output voltage of the RR. At the same time, the improved AVM of the variable parameter does not need to be scanned before running according to the load properties, so it is more concise than the original model. In the controller part, the nonlinear relationship mainly originated from the switching tube controlled by the PWM signal and from the freewheeling diode. Combined with the specific circuit form, analyzing the signal transfer logic solved the problem of signal inconsistency caused by the GCU. In the power generation state of WRSSG, the signal transmission is progressive and the nonlinear relationship of each part cannot be ignored. Moreover, the nonlinear modeling effect of each part directly determines the effectiveness of the WRSSG nonlinear model.

Finally, the nonlinear model proposed in this paper has been compiled and run in RT-LAB real time simulator without time-out, which lays a foundation for the establishment of a hardware-on-loop platform. FEA was also used to verify the accuracy of the system. In the test, the system met the MIL-STD-704F standard and output high power supply quality. The nonlinear model and the presented research results can play a significant role in the state detection and fault diagnosis of future aircraft power generation systems. Based on this model, the hardware-in-the-loop test platform of aircraft power generation systems can greatly reduce the cost of aircraft power generation system state research and shorten research periods. For the main generator inter-turn short-circuit fault and rotary rectifier fault mentioned in the introduction, the fault mechanism can be studied by using the proposed model, and the fault diffusion mechanism can be explored by using the signal transmission logic of the model. Later, the proposed model can also be combined with the power amplifier to carry out partial semi-physical experiments on the aircraft power generation system, and for the expensive part, the model and the simulator can be used to solve the problem. The hardware-in-the-loop test platform based on this model can promote the research of health management and state monitoring of aircraft power generation system, as well as the research of control strategy of aircraft power generation systems. These studies are of great significance for the formation of an aircraft smart grid.

**Author Contributions:** Conceptualization, H.D., Y.L. and T.L.; methodology, H.D.; software, H.D. and P.Z.; validation, H.D. and Y.L.; formal analysis, H.D.; writing—original draft preparation, H.D. All authors have read and agreed to the published version of the manuscript.

**Funding:** This research received no external funding.

**Data Availability Statement:** The data that support the findings of this study are available from the corresponding author upon reasonable request.

**Conflicts of Interest:** The authors declare no conflict of interest.

## References

- Buticchi, G.; Wheeler, P.; Boroyevich, D. The More-Electric Aircraft and Beyond. *Proc. IEEE* **2023**, *111*, 356–370. [[CrossRef](#)]
- Sarlioglu, B.; Morris, C.T. More Electric Aircraft: Review, Challenges, and Opportunities for Commercial Transport Aircraft. *IEEE Trans. Transp. Electrification*. **2015**, *1*, 54–64. [[CrossRef](#)]
- Cano, T.C.; Castro, I.; Rodriguez, A.; Lamar, D.G.; Khalil, Y.F.; Albiol-Tendillo, L.; Kshirsagar, P. Future of Electrical Aircraft Energy Power Systems: An Architecture Review. *IEEE Trans. Transp. Electrification*. **2021**, *7*, 1915–1929. [[CrossRef](#)]
- Sayed, E.; Abdalmagid, M.; Pietrini, G.; Sa’adeh, N.M.; Callegaro, A.D.; Goldstein, C.; Emadi, A. Review of Electric Machines in More-/Hybrid-/Turbo-Electric Aircraft. *IEEE Trans. Transp. Electrification*. **2021**, *7*, 2976–3005. [[CrossRef](#)]
- Robbins, D.; Bobalik, J.; De Stena, D.; Martin, N.; Plag, K.; Rail, K.; Wall, K. F-35 Subsystems Design, Development & Verification. In Proceedings of the 2018 Aviation Technology, Integration, and Operations Conference, Atlanta, GA, USA, 25–29 June 2018; American Institute of Aeronautics and Astronautics: Atlanta, GA, USA, 2018.
- Chen, J.; Wang, C.; Chen, J. Investigation on the Selection of Electric Power System Architecture for Future More Electric Aircraft. *IEEE Trans. Transp. Electrification*. **2018**, *4*, 563–576. [[CrossRef](#)]
- Wang, Y.; Nuzzo, S.; Zhang, H.; Zhao, W.; Gerada, C.; Galea, M. Challenges and Opportunities for Wound Field Synchronous Generators in Future More Electric Aircraft. *IEEE Trans. Transp. Electrification*. **2020**, *6*, 1466–1477. [[CrossRef](#)]
- Madonna, V.; Giangrande, P.; Galea, M. Electrical power generation in aircraft: Review, challenges, and opportunities. *IEEE Trans. Transp. Electrification*. **2018**, *4*, 646–659. [[CrossRef](#)]
- Pang, J.; Liu, W.; Jiao, N.; Wang, J.; Ma, P. Calculation of cross-coupling inductance and electromagnetic torque in wound-rotor synchronous starter/generator. *IEEE Trans. Ind. Electron.* **2019**, *66*, 5115–5123. [[CrossRef](#)]
- Bozhko, S.; Yang, T.; Le Peuedic, J.-M.; Arumugam, P.; Degano, M.; La Rocca, A.; Xu, Z.; Rashed, M.; Fernando, W.; Hill, C.I.; et al. Development of Aircraft Electric Starter–Generator System Based on Active Rectification Technology. *IEEE Trans. Transp. Electrification*. **2018**, *4*, 985–996. [[CrossRef](#)]
- Batzel, T.D.; Swanson, D.C. Prognostic Health Management of Aircraft Power Generators. *IEEE Trans. Aerosp. Electron. Syst.* **2009**, *45*, 473–482. [[CrossRef](#)]
- Nuzzo, S.; Galea, M.; Gerada, C.; Brown, N. Analysis, Modeling, and Design Considerations for the Excitation Systems of Synchronous Generators. *IEEE Trans. Ind. Electron.* **2018**, *65*, 2996–3007. [[CrossRef](#)]
- Sun, C.; Liu, W.; Han, X.; Zhang, X.; Jiao, N.; Mao, S.; Wang, R.; Guan, Y. High-Frequency Voltage Injection-Based Fault Detection of a Rotating Rectifier for a Wound-Rotor Synchronous Starter/Generator in the Stationary State. *IEEE Trans. Power Electron.* **2021**, *36*, 13423–13433. [[CrossRef](#)]
- Jiao, N.; Han, X.; Wei, Z.; Sun, C.; Liang, P.; Liu, W. Online Fault Diagnosis for Rotating Rectifier in Wound-Rotor Synchronous Starter–Generator Based on Geometric Features of Current Trajectory. *IEEE Trans. Ind. Electron.* **2021**, *68*, 2952–2963. [[CrossRef](#)]
- Beltran-Pulido, A.; Aliprantis, D.; Billionis, I.; Munoz, A.R.; Leonardi, F.; Avery, S.M. Uncertainty Quantification and Sensitivity Analysis in a Nonlinear Finite-Element Model of a Permanent Magnet Synchronous Machine. *IEEE Trans. Energy Convers.* **2020**, *35*, 2152–2161. [[CrossRef](#)]
- Yamazaki, K.; Iida, K.; Terai, Y. Fast Estimation of Harmonic Losses Caused by Inverter Carrier in Interior Permanent-Magnet Synchronous Motors by Using Combination of Time- and Frequency-Domain Finite-Element Analyses. *IEEE Trans. Magn.* **2020**, *56*, 1–4. [[CrossRef](#)]
- Cho, S.; Hwang, J.; Kim, C.-W. A Study on Vibration Characteristics of Brushless DC Motor by Electromagnetic-Structural Coupled Analysis Using Entire Finite Element Model. *IEEE Trans. Energy Convers.* **2018**, *33*, 1712–1718. [[CrossRef](#)]
- Shen, M.; Pfister, P.-D.; Tang, C.; Fang, Y. A Hybrid Model of Permanent-Magnet Machines Combining Fourier Analytical Model with Finite Element Method, Taking Magnetic Saturation into Account. *IEEE Trans. Magn.* **2021**, *57*, 1–5. [[CrossRef](#)]
- Shimotani, T.; Sato, Y.; Sato, T.; Igarashi, H. Fast Finite-Element Analysis of Motors Using Block Model Order Reduction. *IEEE Trans. Magn.* **2016**, *52*, 1–4. [[CrossRef](#)]
- JLee, J.-H.; Kwon, Y.-C.; Sul, S.-K. High-Fidelity Induction Motor Simulation Model Based on Finite Element Analysis. *IEEE Trans. Ind. Electron.* **2022**, *69*, 9872–9883.
- Eldeeb, H.H.; Berzoy, A.; Mohammed, O. Stator Fault Detection on DTC-Driven IM via Magnetic Signatures Aided by 2-D FEA Co-Simulation. *IEEE Trans. Magn.* **2019**, *55*, 1–5. [[CrossRef](#)]
- Chen, X.; Wang, J.; Griffo, A. A High-Fidelity and Computationally Efficient Electrothermally Coupled Model for Interior Permanent-Magnet Machines in Electric Vehicle Traction Applications. *IEEE Trans. Transp. Electrification*. **2015**, *1*, 336–347. [[CrossRef](#)]
- Chen, X.; Wang, J.; Sen, B.; Lazari, P.; Sun, T. A High-Fidelity and Computationally Efficient Model for Interior Permanent-Magnet Machines Considering the Magnetic Saturation, Spatial Harmonics, and Iron Loss Effect. *IEEE Trans. Ind. Electron.* **2015**, *62*, 4044–4055. [[CrossRef](#)]
- Chow, M.-Y.; Thomas, R.J. Neural network synchronous machine modeling. In *IEEE International Symposium on Circuits and Systems*; IEEE: Portland, OR, USA, 1989; pp. 495–498.
- Sudhoff, S.; Wasynczuk, O. Analysis and average-value modeling of line-commutated converter-synchronous machine systems. *IEEE Trans. Energy Convers.* **1993**, *8*, 92–99. [[CrossRef](#)]

26. Wang, S.; Ruan, X.; He, Y.; Lin, Z.; Zhang, C.; Wu, D. Small-Signal Impedance Modeling and Analysis of Variable-Frequency AC Three-Stage Generator for More Electric Aircraft. *IEEE Trans. Power Electron.* **2023**, *38*, 206–216. [[CrossRef](#)]
27. Areerak, K.-N.; Wu, T.; Bozhko, S.V.; Asher, G.M.; Thomas, D.W.P. Aircraft Power System Stability Study Including Effect of Voltage Control and Actuators Dynamic. *IEEE Trans. Aerosp. Electron. Syst.* **2011**, *47*, 2574–2589. [[CrossRef](#)]
28. Jatskevich, J.; Pekarek, S.; Davoudi, A. Parametric Average-Value Model of Synchronous Machine-Rectifier Systems. *IEEE Trans. Energy Convers.* **2006**, *21*, 9–18. [[CrossRef](#)]
29. Jatskevich, J.; Pekarek, S.D.; Davoudi, A. Fast Procedure for Constructing an Accurate Dynamic Average-Value Model of Synchronous Machine-Rectifier Systems. *IEEE Trans. Energy Convers.* **2006**, *21*, 435–441. [[CrossRef](#)]
30. Li, J.; Zhang, Z.; Lu, J.; Liu, Y.; Chen, Z. Design and Characterization of a Single-Phase Main Exciter for Aircraft Wound-Rotor Synchronous Starter–Generator. *IEEE Trans. Magn.* **2018**, *54*, 1–5. [[CrossRef](#)]
31. Jiao, N.; Li, Z.; Mao, S.; Sun, C.; Liu, W. Aircraft Brushless Wound-Rotor Synchronous Starter–Generator: A Technology Review. *IEEE Trans. Power Electron.* **2023**, *38*, 7558–7574. [[CrossRef](#)]

**Disclaimer/Publisher’s Note:** The statements, opinions and data contained in all publications are solely those of the individual author(s) and contributor(s) and not of MDPI and/or the editor(s). MDPI and/or the editor(s) disclaim responsibility for any injury to people or property resulting from any ideas, methods, instructions or products referred to in the content.